

UDK: 675.017.5; 581.135.5

## Improving Thermoelectric Properties of p-type (BiSb)<sub>2</sub>(TeSe)<sub>3</sub> Single Crystal by Zr Doping

Emina Požega<sup>1\*</sup>, Nikola Vuković<sup>2</sup>, Lidija Gomidželović<sup>1</sup>, Miloš Janošević<sup>1</sup>, Milenko Jovanović<sup>1</sup>, Saša Marjanović<sup>3</sup>, Milijana Mitrović<sup>3</sup>

<sup>1</sup>Mining and Metallurgy Institute Bor, Zeleni Bulevar 35, 19210 Bor, Serbia;

<sup>2</sup>Municipality of Kladovo, Kralja Aleksandra 35, 19320 Kladovo, Serbia

<sup>3</sup>University of Belgrade, Technical Faculty Bor, VJ 12, 19210 Bor, Serbia

---

### Abstract:

*In order to study the effect of Zr doping on the thermoelectric properties of p-type Bi<sub>10.17</sub>Sb<sub>30.72</sub>Zr<sub>0.35</sub>Te<sub>58.28</sub>Se<sub>0.48</sub> single crystal, an ingot was prepared by Bridgman method. Cut and cleaved samples from different regions of ingot were characterized by a Hall Effect based on the Van der Pauw method. The first measurements were conducted with four ohmic contacts at room temperature and the obtained results were presented in our investigation, earlier. Also, high charge carriers mobility was obtained on the sample with silver contacts at the temperature of liquid nitrogen. Single crystal was characterized by Seebeck coefficient (S), conductivity (κ) and resistivity (ρ) measurements as a function of temperature in the range of 40-320°C by a home-made impedance meter. The prepared single crystal has a figure of merit (Z) of 1.22 x 10<sup>-3</sup> K<sup>-1</sup> at 300°C.*

**Keywords:** Hall Effect; Thermoelectric properties; Bridgman method; Single crystal.

---

## 1. Introduction

To improve thermoelectric properties of a material, the carrier concentration needs to be optimized first. The increase of carrier concentration usually results in degraded carrier mobility, which restricts the enhancement in thermoelectric performance.

Electrical properties of semiconductors strongly depend on the carrier concentration, carrier mobility, crystal structure, and point defects [1]. Defects significantly degrades properties [2,3]. Semiconductor properties can be improved and modified by forming ternary, quaternary etc. compounds.

Actually used thermoelectric (TE) materials are: Bi-Sb; Bi<sub>2</sub>Te<sub>3</sub>-Sb<sub>2</sub>Te<sub>3</sub>; (Bi,Sb)<sub>2</sub>(Te,Se)<sub>3</sub>; PbTe; Te-Ag-Ge-Sb; Si-Ge). Their performance bound to a stagnant ZT~1 which had not much changed up to 1990 [4].

The best TE materials near room temperature are p-type Bi<sub>2-x</sub>Sb<sub>x</sub>Te<sub>3</sub> and n-type Bi<sub>2</sub>Te<sub>3-y</sub>Se<sub>y</sub>, which are widely used for cooling applications. The compositions of commercialized p-type and n-type ingots are near Bi<sub>0.5</sub>Sb<sub>1.5</sub>Te<sub>3</sub> and Bi<sub>2</sub>Te<sub>2.7</sub>Se<sub>0.3</sub> (which is optimum composition for thermoelectric cooling devices), respectively, and their ZT values are about 1.0 at 27°C [5-7].

Much effort has been made to raise Z of materials based on Bi<sub>2</sub>Te<sub>3</sub> by doping in various fabrication processes [1, 8-10]. Poudel et al. showed that a ZT peak of 1.4 at 100°C

---

<sup>\*</sup> Corresponding author: emina.pozega@irmbor.co.rs

can be achieved in a p-type nanocrystalline BiSbTe bulk alloy [6]. Se-doped n-type  $\text{Bi}_2\text{Te}_{2.7}\text{Se}_{0.3}$  single crystal was reported with maximum figure of merit,  $ZT \sim 1.04$  at  $125^\circ\text{C}$  [10].

Fang [11] investigated effects of Ce, Y, and Sm doping on thermoelectric properties of  $\text{Bi}_2\text{Te}_3$  alloy. Results showed that Ce is a superior dopant and also significant effects of Ce, Y, and Sm doping on the morphologies of the synthesized nanopowders and thermoelectric properties. Figure of merit ( $ZT$ ) of  $\text{Ce}_{0.2}\text{Bi}_{1.8}\text{Te}_3$  were improved and reaches 1.29 at  $125^\circ\text{C}$ .

To enhance the performance of bismuth telluride based TE alloys Mosen developed composite TE materials [12]. Lowering conductivity without compromising the power factor  $S^2\sigma$  is a challenge in Bi-Sb-Te-Se alloys. For a material is difficult to possess simultaneously good electrical conductivity which is characteristic of metals and bad thermal conductivity which is characteristic of insulators [13-17]. The BiSbTeSe solid solution attracted attention because of its promising thermoelectric properties for near room temperature applications. Thermoelectric properties of  $\text{Bi}_{2-x}\text{Sb}_x\text{Te}_{3-y}\text{Se}_y$  compositions with a  $ZT \sim 0.8$  at  $-48^\circ\text{C}$  indicate that this type of materials can be used for cooling [2].  $\text{Bi}_{0.5}\text{Sb}_{1.5}\text{Te}_{2.7}\text{Se}_{0.3}$  (BSTS) high-quality quaternary alloy with maximum  $ZT$  value of 0.95 at  $230^\circ\text{C}$  was successfully synthesized by high pressure and high temperature method (HPHT) [18].

Research on thermoelectric materials is being carried out in Serbia also [19-33]. The aim of the present study is to characterize properties of BiSbTeSe single crystal doped with Zr and to examine the possibility of using these materials in thermoelectric devices. Our material has a  $ZT$  of 0.7 at  $300^\circ\text{C}$ . Conventional  $\text{Bi}_2\text{Te}_3$  based materials have a peak  $ZT$  of about 0.25 at  $250^\circ\text{C}$  [6]. The high  $ZT$  in the  $300^\circ\text{C}$  range makes investigated single crystal attractive for segmented thermoelectric devices that operate at high temperatures.

## 2. Materials and Experimental Procedures

High purity Bi (Sigma – Aldrich, 99.999%), Sb (Koch Light Laboratories LTD, 99.99%), Zr (KEFO, 99.98%), Te (Sigma – Aldrich, 99.99%) and Se (Alfa Aesar, 99.99%) were weighed for the composition of  $\text{Bi}_{10.17}\text{Sb}_{30.72}\text{Zr}_{0.35}\text{Te}_{58.28}\text{Se}_{0.48}$  crystal. Single crystal doped with Zr was synthesized by Bridgman method [34]. The crystal growth was achieved in a closed quartz ampoule under a pressure of  $10^{-5}$  Pa. Before the synthesis beginning, it was necessary to prepare a quartz ampoule. One end of the quartz ampoule is heated to obtain a semi-open tube. The ampoule is coated on the inside with a thin film to eliminate wetting of the ampoule with the material in the molten state. A thin film on the inside of the ampoule prevented the batch in the molten state from chemically reacting with the material from which the ampoule was made in which the single crystal solidified. On the underside, the ampoule was conical in shape for easier germ formation. In this way, only a small part of the melt was sub cooled at the top of the conical capillary. During growth through the capillary, one germ with the most favorable orientation overcame the others. A single crystal formed in a capillary was used as a seed for crystallization.

The ampoule was heated to the synthesis temperature for 3 days. Then the ampoule was on a stable temperature gradient for 14 days. It was then cooled naturally to room temperature.

The obtained single crystal was characterized by the Hall measurements (mobility ( $\mu$ ), bulk carrier concentration ( $n_b$ ), sheet carrier concentration ( $n_s$ ), resistivity ( $\rho$ ), conductivity ( $\sigma$ ), Hall coefficient ( $R_H$ )) and thermoelectric measurements (Seebeck coefficient ( $S$ ), conductivity ( $k$ ), resistivity( $\rho$ )). The actual sample composition was determined using the Energy Dispersive X-ray Spectroscopy (EDS) analysis [34]. Hall measurements were performed on a Hall Effect measurement system (Ecopia, HMS-3000) at temperature of liquid nitrogen at different electric currents for an applied magnetic field strength of 0.37 T. Software for Hall Effect measurement system (Ecopia, HMS-3000) automatically calculated

bulk and sheet carrier concentration, resistivity, conductivity and Hall coefficient. Calculations were done on the basis of voltage obtained by Van der Pauw laws and input data was entered into the software (sample thickness  $D$ , current intensity  $I$ , the magnetic induction of permanent magnet  $B$ ). Data from Hall measurements at temperature of liquid nitrogen was collected using silver contacts. The measured ingot samples were cut and cleaved from different regions with cutting route which was perpendicular ( $\perp$ ) and for cleaved samples parallel ( $\parallel$ ) to the plane of crystallisation. In the following text these samples will be marked as 8/5 ( $\parallel$ ), 8/6 ( $\perp$ ) and 8/8 ( $\parallel$ ), respectively. Samples cut perpendicular ( $\perp$ ) to the growth of the ingot were in the form of discs and samples cleaved parallel ( $\parallel$ ) to the plane of crystallisation were of square cross-section. Cut samples were then highly mechanically polished. The measured samples were cleaned in acetone before they are used for measurements.

Measurements of thermoelectric properties were carried out by home-made impedance meter based on the "Lagre  $\Delta T$  method" [35] with temperature range from 40 to 320°C. Home-made impedance meter simultaneously measured all three thermoelectric parameters, Seebeck coefficient, conductivity and resistivity. The measurement process was performed in vacuum of  $10^{-2}$  to  $10^{-3}$  Pa on sample with a height of about 11.72 mm and a diameter of 9.15 mm and took at least 15 hours.

TE characteristics of sample, resistivity ( $\rho$ ), Seebeck coefficient ( $S$ ) and conductivity ( $\kappa$ ) were used to determine figure of merit,  $ZT$ .  $T$  is absolute temperature. The sample dimensionless figure of merit  $ZT$  was calculated according to the expression:

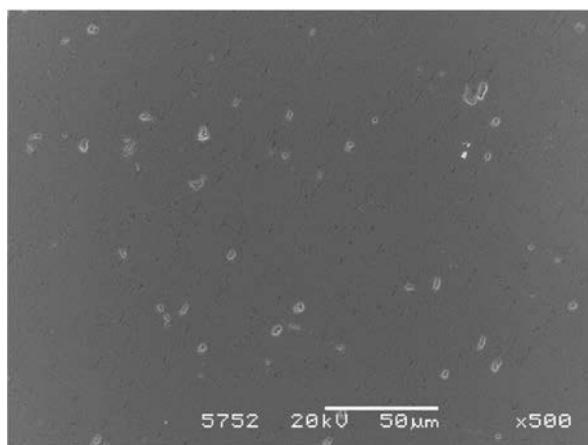
$$ZT = S^2 \cdot T / \rho \cdot \kappa \quad (1)$$

Thermoelectric measurements were taken for decreasing temperature and in the directions perpendicular to the 001 plane.

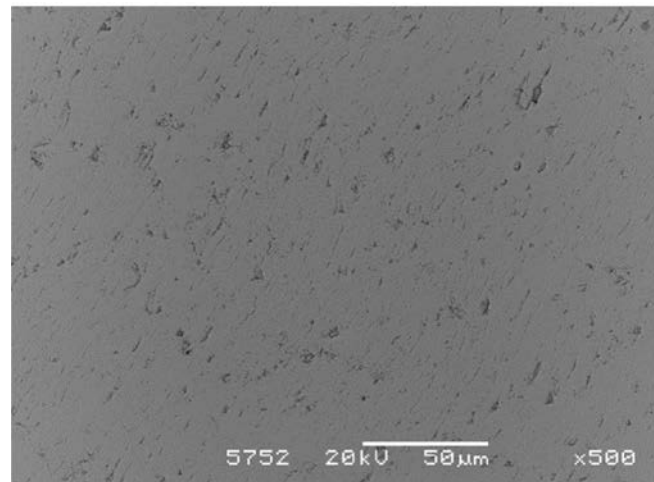
### 3. Results and Discussion

Bismuth, antimony, zirconium, tellurium and selenium are merged in a stoichiometric relationship 2:3, namely with given compound formula of  $\text{Bi}_{10.17}\text{Sb}_{30.72}\text{Zr}_{0.35}\text{Te}_{58.28}\text{Se}_{0.48}$ . The elemental composition of the compound obtained by energy dispersive spectrometry (EDS) analysis [34] made it possible to obtain empirical formula. The obtain empirical formula does not deviate from the given compound formula.

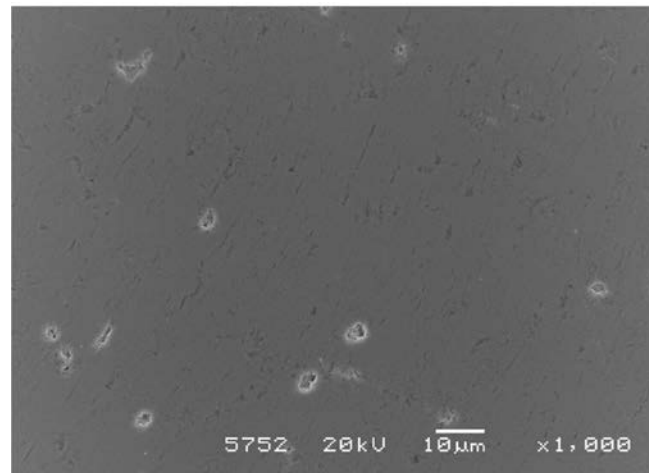
Secondary and backscattered electron image (SEI and BEI) shows the chemical homogeneity of the sample as seen in the Figs 1–4.



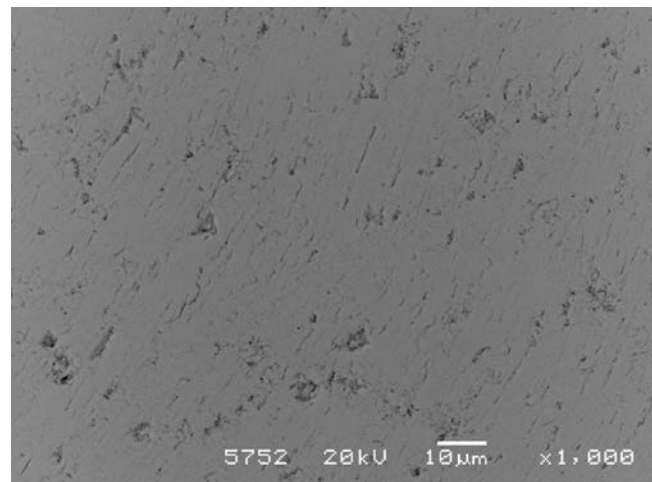
**Fig. 1.** Secondary electron image (SEI) of  $\text{Bi}_{10.17}\text{Sb}_{30.72}\text{Zr}_{0.35}\text{Te}_{58.28}\text{Se}_{0.48}$ .



**Fig. 2.** Backscattered electron images BEI  $\text{Bi}_{10.17}\text{Sb}_{30.72}\text{Zr}_{0.35}\text{Te}_{58.28}\text{Se}_{0.48}$ .

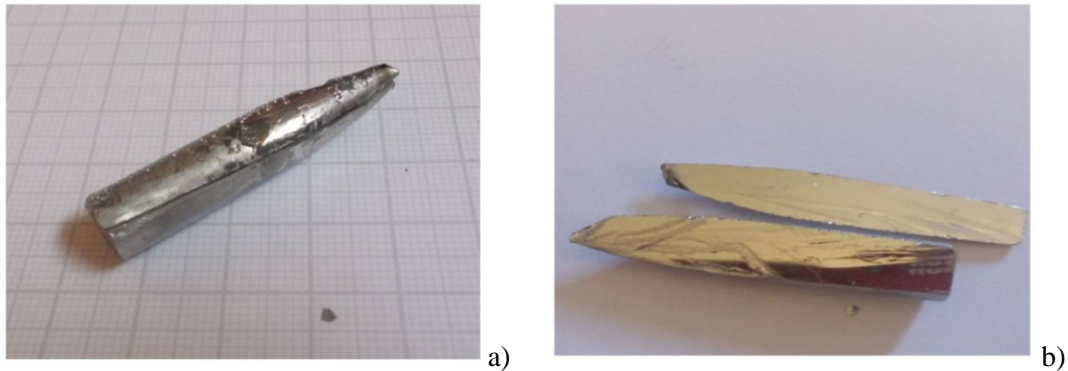


**Fig. 3.** Secondary electron image (SEI) of  $\text{Bi}_{10.17}\text{Sb}_{30.72}\text{Zr}_{0.35}\text{Te}_{58.28}\text{Se}_{0.48}$ .



**Fig. 4.** Backscattered electron images (BEI) of  $\text{Bi}_{10.17}\text{Sb}_{30.72}\text{Zr}_{0.35}\text{Te}_{58.28}\text{Se}_{0.48}$ .

In Figs 1 and 3 shows the sample microstructure secondary electron image (SEI), so that the pores are better visible. Figs 2 and 4 are BEI images backscattered electron image, so they carry information about the chemical composition (phases with a higher atomic number average,  $Z$ , reject more electrons, so they are brighter, and phases with a smaller atomic number average,  $Z$ , reject less electrons, so they are darker in the figures). The porosity of the sample can be clearly seen from the microstructures and that the sample is single-phase (darker areas in the BEI images are pores).



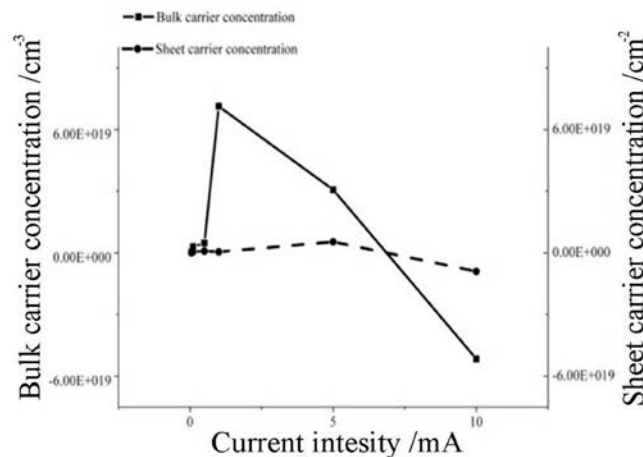
**Fig. 5** Cleaved ingot in the crystallization direction a) i b).

Fig. 5a) displayed the look of the obtained  $\text{Bi}_{10.17}\text{Sb}_{30.72}\text{Zr}_{0.35}\text{Te}_{58.28}\text{Se}_{0.48}$  single crystal. The obtained crystal could be easily cleaved along the (001) plane and it has a shiny surface, Fig. 5b).

### 3.1 Hall Effect measurements at temperature of liquid nitrogen

Hall effect measurements at a temperature of liquid nitrogen were carried out with 0.05; 0.1; 0.5; 1; 5 and 10 mA current intensity. Square cross-section sample 8/5 (II) and 8/8 (II) was with thickness of 1.75 mm and circular cross-section sample 8/6 ( $\perp$ ) was with thickness of 2.25 mm.

All calculated data from Hall measurements at temperature of liquid nitrogen for samples: 8/5(II), 8/6 ( $\perp$ ) and 8/8 (II) are presented in Figs 6-13.



**Fig. 6.** Dependence of bulk and sheet carrier concentration from current intensity for sample 8/5 (II) at temperature of liquid nitrogen.

Dependence of bulk and sheet carrier concentration from current intensity for sample 8/5 (II) at temperature of liquid nitrogen is displayed in Fig. 6. Sheet carrier concentration is fairly constant and was found to be  $10^{18} \text{ cm}^{-2}$ . Bulk carrier concentrations at current intensity of 0.05 mA, 0.1 mA and 0.5 mA are  $n_b = 3.342 \times 10^{17} \text{ cm}^{-3}$ ,  $n_b = 3.027 \times 10^{18} \text{ cm}^{-3}$ ,  $n_b = 4.751 \times 10^{18}$  respectively. At current intensity of 1 mA bulk carrier concentration increases to value of  $71.375 \times 10^{18}$ . Thereafter bulk carrier concentration decreases as current intensity increases.

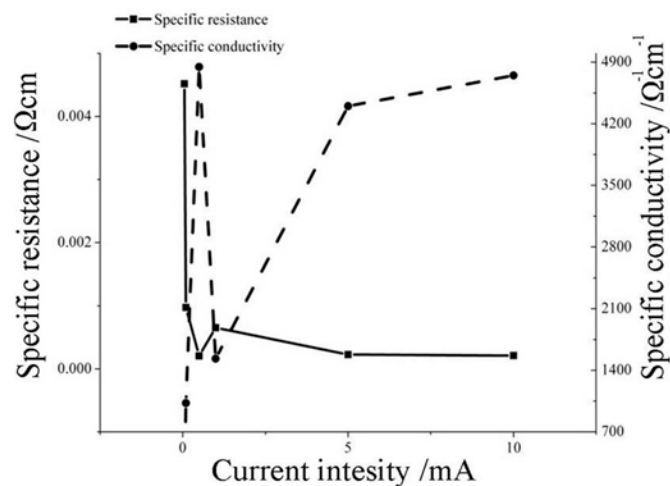


**Fig. 7.** Dependence of specific resistivity and conductivity from current intensity for sample 8/5 (II) at temperature of liquid nitrogen.

The resistivity of sample 8/5 (II) shown in Fig. 7 decreases as current intensity increases from 0.05 to 5 mA and is fairly constant in range of 5–10 mA. The plot of the conductivity dependence from current intensity for sample 8/5 (II) at temperature of liquid nitrogen is shown in the same Fig. 7. As it can be seen the conductivity increases as current intensity increases from 0.05 to 5 mA. At current intensity of 1 mA specific conductivity is  $\sigma = 1.533 \times 10^3 \Omega^{-1} \text{ cm}^{-1}$ . After that specific conductivity again increases.

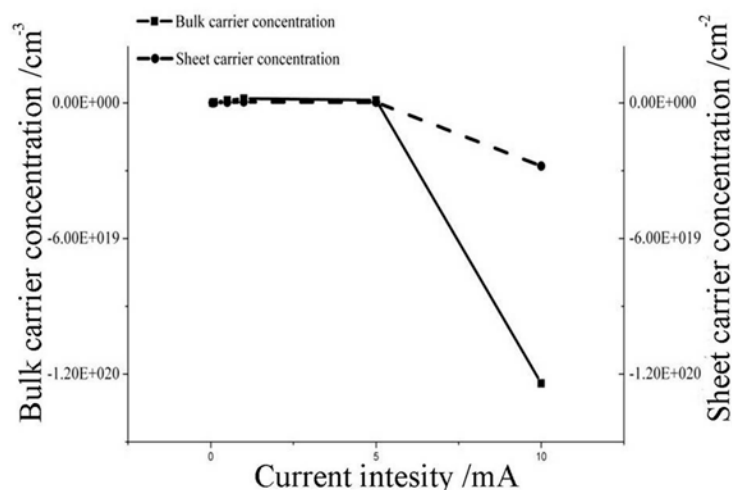


**Fig. 8.** Dependence of bulk and sheet carrier concentration from current intensity for sample 8/6 (I) at temperature of liquid nitrogen.

Dependence of bulk and sheet carrier concentration from current intensity for sample 8/6 ( $\perp$ ) at temperature of liquid nitrogen is displayed in Fig. 8. Bulk and sheet carrier concentration are fairly constant in range of 0.05–5 mA. The figure shows that bulk and sheet carrier concentration is in the range of  $10^{16}$ – $10^{20}$   $\text{cm}^{-3}$ .

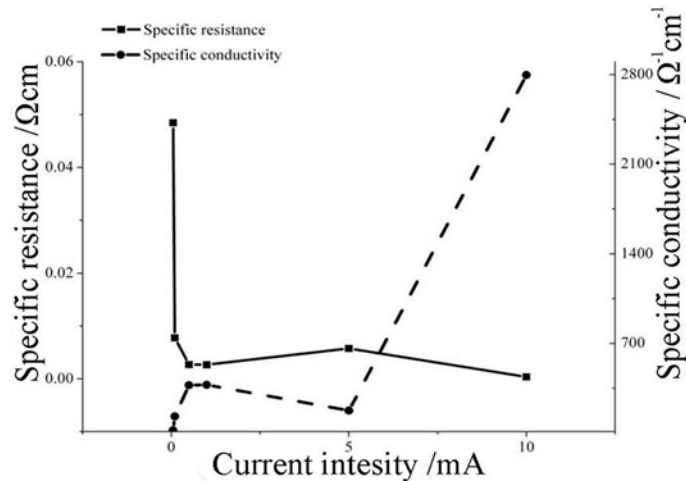


**Fig. 9.** Dependence of specific resistance and conductivity from current intensity for sample 8/6 ( $\perp$ ) at temperature of liquid nitrogen.

It may be noted that the specific resistance decreases as current intensity increases from 0.05 to 1 mA (Fig. 9). Specific resistance is fairly constant in range of 1–10 mA. Specific conductivity increases as current intensity increases except for current intensity of 5 mA.

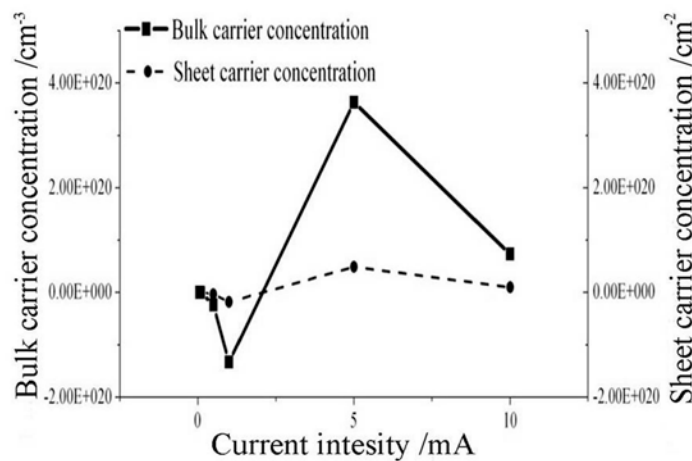


**Fig. 10.** Dependence of bulk and sheet carrier concentration from current intensity for sample 8/8 (||) at 77 K.

In Fig. 10 is displayed dependence of bulk and sheet carrier concentration from current intensity for sample 8/8 (||) at 77 K. Sheet carrier concentration is fairly constant in range of 0.05–10 mA ( $10^{16}$ – $10^{19}$   $\text{cm}^{-2}$ ) while values of bulk carrier concentration vary in the same range.

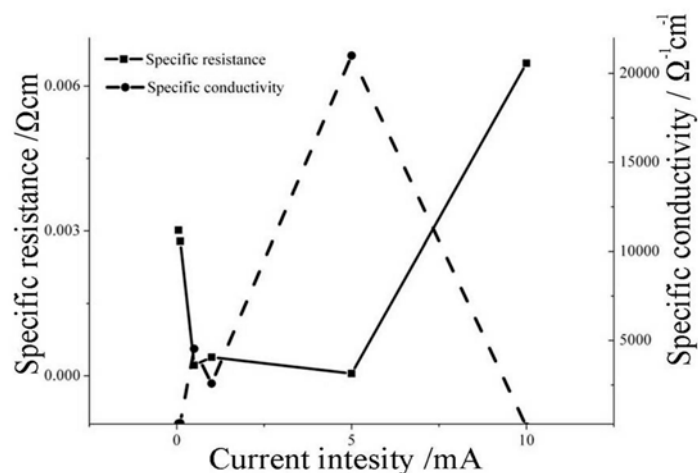


**Fig. 11.** Dependence of specific resistance and conductivity from current intensity for sample 8/8 (II) at temperature of liquid nitrogen.

The measurement results of specific resistance and conductivity dependence from current intensity for sample 8/8 (II) at temperature of liquid nitrogen are shown in Fig. 11. It can be seen that the resistance decreases (except from interval of 5-10 mA current intensity) with current intensity showing metallic character of the material. A little deviation in derived measurement results of specific resistance, conductivity, bulk and sheet carrier concentration can be contributed to interval time between measurements.

The obtained results of specific conductivity for samples 8/5 (II) and 8/8 (II) are higher than for cut sample 8/6 (⊥).

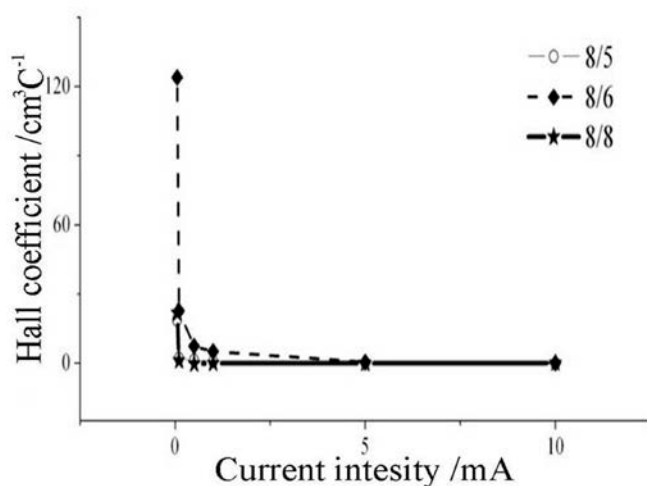


**Fig. 12.** The variation of Hall coefficient  $R_H$  with current for samples: 8/5 (II), 8/6 (⊥) and 8/8 (II) at temperature of liquid nitrogen.

The variation of the Hall coefficient  $R_H$  at 77K with current is shown in Fig. 12. It is seen that the Hall coefficient is fairly constant in range of current value 2.5–10 mA. Values of Hall coefficient is negative for sample 8/5 (II) at 10 mA and for sample 8/8 (II) at 0.5 and 1 mA which can be contributed to interval time between measurements or deviation from stoichiometry [36]. The positive value of the Hall coefficient points out that BiSbTeSe single crystal doped with Zr is p-type and the majority charge carriers are holes.



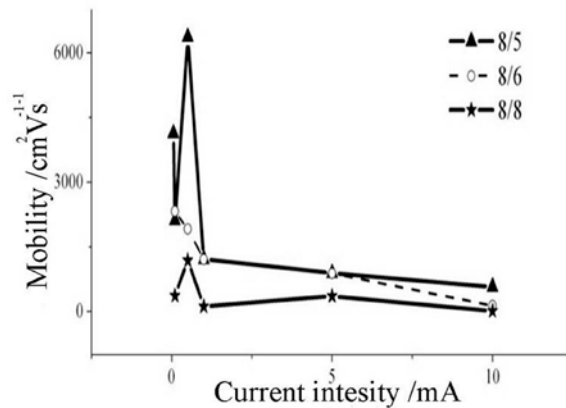


**Fig. 13.** The variation of mobility with current for samples: 8/5 (▲), 8/6 (○) and 8/8 (★) at temperature of liquid nitrogen.

Fig. 13 shows results of mobility measurements for all three samples. It can be seen that the mobility of each sample decreases as current increases in range of current value 0.05 – 1 mA and are higher than theoretical mobility value of p type  $\text{Bi}_2\text{Te}_3$  and reported value of Bi-Sb-Te-Se quaternary system [37-39]. In range of 1–10 mA mobility is fairly constant for all three samples.

If obtained mobility value for sample 8/5 (▲) at 0.05 mA is disregarded, obtained curves for 8/5 (▲) and 8/8 (★) samples are similar. Mobility  $\mu$  ( $\text{cm}^2\text{V}^{-1}\text{s}^{-1}$ ), varies from  $4.134 \times 10^3$ ,  $2.119 \times 10^3$ ,  $6.367 \times 10^3$ ,  $1.218 \times 10^3$ ,  $8.950 \times 10^2$  and  $5.750 \times 10^2$  for sample 8/5 (▲) at 77 K. For sample 8/6 (○) mobility is in range  $2.325 \times 10^3$  -  $1.406 \times 10^2 \text{ cm}^2\text{V}^{-1}\text{s}^{-1}$ , while for sample 8/8 (★) at 77 K measured values are between  $7.227 \times 10^3 \text{ cm}^2\text{V}^{-1}\text{s}^{-1}$  and  $1.309 \times 10^1 \text{ cm}^2\text{V}^{-1}\text{s}^{-1}$ . High value of mobility may be attributed to the presence of fewer defects in single crystal.

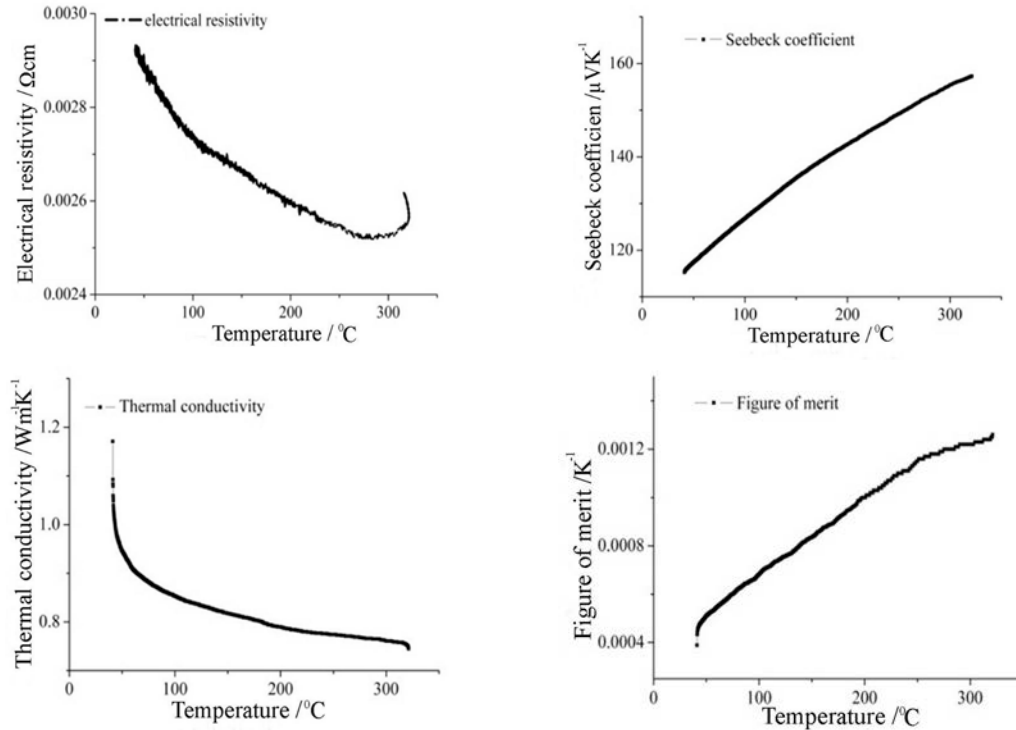
### 3.2 Thermoelectric properties

Preliminary results of thermoelectric properties in the temperature interval from 40°C to 320°C are given in Fig. 14. Figure shows the temperature dependence of resistivity ( $\rho$ ), Seebeck coefficient ( $S$ ), conductivity ( $k$ ) and figure of merit ( $ZT$ ) of sample. A TE characteristic was measured to define quality. These properties strongly depend on carrier concentration, mobility, crystal structure and defects in the crystal structure.

Resistivity ( $\rho$ ) as a function of temperature ( $T$ ) is displayed in Fig. 14a. The  $R$ - $T$  curve demonstrates resistivity decrease as temperatures increase. This trend has been kept up to about 300°C. Thereafter resistivity increases. Resistivity is inversely proportional to the carrier mobility ( $\mu$ ). Higher carrier mobility will result in lower resistivity, so that may result in decrease of resistivity to about 300°C.

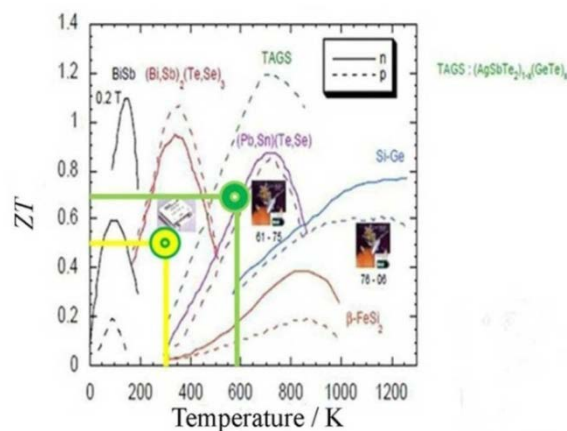
Temperature dependence of Seebeck coefficient ( $S$ ) in temperature range from 40°C to approximately 300°C is shown in Fig. 14b. The sample showed increase of  $S$  with temperature from  $120 \mu\text{V}^\circ\text{C}^{-1}$  at 40°C to  $155 \mu\text{V}^\circ\text{C}^{-1}$  at 320°C. Seebeck coefficient had a positive sign over the whole investigated temperature range which indicates p-type of conduction (major conductivity carriers are holes) which is in agreement with the Hall coefficient. The variation in conductivity ( $\kappa$ ) with temperature of studied sample is shown in Figure 14c. The analyzed sample had conductivity of  $0.8 \text{ Wm}^{-1}\text{K}^{-1}$  approximately. Over the whole temperature range, the conductivity is much lower than in  $\text{Bi}_2\text{Te}_3$  based alloys [40]. A marked decrease in the conductivity from  $0.98$  to  $0.78 \text{ Wm}^{-1}\text{K}^{-1}$  was observed at high temperatures (300°C). Decrease in the conductivity with temperature (Fig. 14c) may be

attributed to the presence of only one type of carrier which takes part in the conductivity [41-44].





**Fig. 14.** Temperature dependence of resistivity (a), Seebeck coefficient (b), conductivity (c) and figure of merit (d) for sample BiSbTeSe doped with Zr.

Figure of merit was calculated using measured values for resistivity, Seebeck coefficient and conductivity. Its temperature dependence is presented in Fig. 14d. The  $ZT$  peak in Figure 14d is about 0.8 at 300°C, which is significantly greater than  $\text{Bi}_2\text{Te}_3$  based alloys. The  $ZT$  value of the  $\text{Bi}_2\text{Te}_3$  based alloys starts to drop above 75°C and is below 0.25 at 250°C [6]. The peak of dimensionless figure of merit ( $ZT$ ) of  $\text{Bi}_2\text{Te}_3$  based n-type single crystals is about 0.85 in the  $ab$  plane at room temperature [43]. However,  $ZT$  values for p-type BiSbTeSe single crystal doped with Zr are still above 0.8 at 300°C (Fig. 14d).



**Fig. 15.** Thermoelectric figure of merit at different temperatures [46, 47] and our investigation.

**Note:**  obtained result of thermoelectric figure of merit in our investigation,  $ZT=0.69$ , for p-type  $\text{Bi}_{10.17}\text{Sb}_{30.72}\text{Zr}_{0.35}\text{Te}_{58.28}\text{Se}_{0.48}$  single crystal at 573 K

 value of thermoelectric figure of merit,  $ZT=0.5$ , for p-type  $\text{Bi}_2\text{Te}_3$  single crystal at 300 K [38].

#### 4. Conclusion

The possibility of producing high quality BiSbTeSe single crystal doped with Zr using the Bridgman method was examined. Single crystal was successfully prepared. Obtained crystal ingot of 80 mm in length and of 9.2 mm in diameter cleaved easily along the (001) planes. Measurements of the Hall Effect and thermoelectric properties indicate that bulk sample was of p-type conductivity, suggesting that major conductivity carriers were holes. The mobility of major carriers varies from  $5.750 \times 10^2$  to  $6.367 \times 10^3$  for sample 8/5 (II). These values of mobility correspond to an increase of nearly 50% from the usual value of mobility for commercial  $\text{Bi}_2\text{Te}_3$  sample. Influence of major charge carriers concentration on structural defects and impurities was lower due to optimal carrier concentration. The resistivity ( $\rho$ ), conductivity ( $k$ ) and Seebeck coefficient ( $S$ ) were measured simultaneously in temperature range from 40°C to 320°C. The minimum conductivity was observed to be  $0.78 \text{ Wm}^{-1}\text{K}^{-1}$  at 300°C. This value is improvement compared with the conductivity of the commercial  $\text{Bi}_2\text{Te}_3$  materials [25]. It was found that figure of merit ( $Z$ ) increases with temperature. The highest figure of merit ( $Z$ ),  $1.22 \times 10^{-3} \text{ K}^{-1}$  at 300°C, was obtained for single crystal BiSbTeSe sample doped with Zr confirming that even small concentration of Zr significantly influences thermoelectric properties of BiSbTeSe single crystal.

The experimental measurements of thermoelectric properties, including Seebeck coefficient, resistivity, conductivity, and figure of merit have shown that fabricated bulk thermoelectric material exhibits high performances for thermoelectric applications.

#### Acknowledgments

Authors wishes to thank Professor Academician Pantelija Nikolić<sup>†</sup> on big and selfless efforts and for his assistance in all stages of doctoral thesis preparation. As well, authors wishes to thank Stevan Vujatović<sup>†</sup>, a specialized technician, for manufacturing high-quality monocrystal ingots, Professor PhD Slavko Bernik from Jozef Stefan Institute, Department of Nanostructured Materials, for measurements of thermoelectric properties, Professor PhD Ljiljana Živanov, full professor at the Department of Electronics, Department of Energy, Electronics and Telecommunications, Faculty of Technical Sciences (FTN), University of Novi Sad and Professor PhD Milan Radovanović, to help with Hall Effect measurement system. The research presented in this paper was done with the financial support of the Ministry of Science, Technological Development and Innovation of the Republic of Serbia, within the financing of scientific research work in the Institute of Mining and Metallurgy Bor, according to the Contract No. 451-03-47/2023-01/200052.

#### 5. References

1. B. Jariwala, D. Shah, N. M. Ravindra, J. Electron. Mater., 44(6) (2015) 1509.
2. A. H. Ma, C. Bao, Sci. Sintering, 53 (3) (2021) 387.

3. A. B. Kulkarni, S. N. Mathad, *Sci. Sintering*, 53 (3) (2021) 407.
4. G. Rogl, D. Setman, E. Schafner, J. Horáky, M. Kerber, M. Zehetbauer, M. Falmbigl, P. Rogl, E. Bauer, *Proceedings of NATO advanced research workshop on new materials for thermoelectric applications: theory and experiment*, Eds. V. Zlatić and A. C. Hewson Hvar, Croatia, 2011, p. 81-92.
5. H. Mun, K. H. Lee, S. J. Kim, J. Y. Kim, J. H. Lee, J. H. Lim, H. J. Park, J. W. Roh, S. W. Kim, *Mater.*, 8 (2015) 959.
6. B. Poudel, Q. Hao, Y. Ma, Y. Lan, A. Minnich, B. Yu, X. Yan, D. Wang, A. Muto, D. Vashaee, *Sci.*, 320 (2008) 634.
7. J. Snyder, E. Toberer, *Nat. Mater.*, 7 (2008) 105.
8. X. Yan, B. Poudel, Y. Ma, W. Liu, G. Joshi, H. Wang, Y. Lan, D. Wang, G. Chen, Z. Ren, *Nano Lett.*, 10 (2010) 3373.
9. W. J. Xie, J. He, H. J. Kang, X. F. Tang, S. Zhu, M. Laver, S. Y. Wang, R. D. Cople, C. M. Brow, Q. J. Zhang, T. M. Tritt, *Nano Lett.*, 10 (2010) 3283.
10. X. B. Zhao, X. H. Ji, Y. H. Zhang, T. J. Zhu, J. P. Tu, X. B. Zhang, *Appl. Phys. Lett.*, 86 (2005) 062111.
11. F. Wu, H. Song, J. Jia, X. Hu, *Prog. Nat. Sci.: Mater. Int.*, 23(4) (2013) 408.
12. M. K. Khorasgani, *Synthesis and characterization of bismuth telluride – based nanostructured thermoelectric composite materials*. PhD thesis, Université de Montréal, École Polytechnique de Montréal, 2014.
13. Rui-di Li, Tie-chui Yuan, Xiao-jun Liu, Ji-wei Wang, H. Wu, Fan-hao Zeng, X. Zhou, *Trans. Nonferrous Met. Soc. China*, 27 (2017) 1594.
14. N. Liu, Xiao-jing Yang, Z. Yu, L. Zhao, *Trans. Nonferrous Met. Soc. China*, 2020, 30: 181-190.
15. N. Liu, Xiao-jing Yang, Z. Yu, L. Zhao, *Trans. Nonferrous Met. Soc. China*, 2020, 30: 181-190.
16. E. Požega, S. Ivanov, Z. Stević, Lj. Karanović, R. Tomanec, L. Gomidželović, A. Kostov, *Trans. Nonferrous Met. Soc. China*, 25 (2015) 3279.
17. N. Liu, Xiao-jing Yang, Z. Yu, L. Zhao, *Trans. Nonferrous Met. Soc. China*, 30 (2020) 181.
18. X. Guo, J. Qin, X. Jia, MA, H. Jia, *J. Alloys Compd.*, 705 (2017) 363.
19. H. I. Elswie, Z. Ž. Lazarević, V. Radojević, M. Gilić M. Rabasović, D. Šević, N. Ž. Romčević, *Sci. Sintering*, 48 (2016) 333.
20. R. M. Abozaid, Z. Ž. Lazarević, V. Radojević, M. S. Rabasović, D. Šević, M. D. Rabasović, N. Ž. Romčević, *Sci. Sintering*, 48 (2018) 445.
21. M. V. Nikolić, D. L. Sekulić, N. Nikolić, M. P. Slankamenac, O. S. Aleksić, H. Danninger, E. Halwax, V. B. Pavlović, P. M. Nikolić, *Sci. Sintering*, 45(3) (2013) 281.
22. N. Nikolić, D. L. Sekulić, O. S. Aleksić, M. N. Mitrić, T. B. Ivetić, V. B. Pavlović, P. M. Nikolić, *Sci. Sintering*, 44(3) (2013) 307.
23. N. N. Obradović, M. V. Nikolić, N. Nikolić, S. Z. Filipović, M. N. Mitrić, V. B. Pavlović, P. M. Nikolić, A. R. Đorđević, M. M. Ristić, *Sci. Sintering*, 44(1) (2012) 65.
24. P. M. Nikolić, S. S. Vujatović, T. B. Ivetić, M. V. Nikolić, O. G. Cvetković, O. S. Aleksić, V. D. Blagojević, G. O. Branković, N. Nikolić, *Sci. Sintering*, 42(1) (2010) 45.
25. T. B. Ivetić, M. V. Nikolić, M. P. Slankamenac, M. B. Živanov, D. M. Minić, P. M. Nikolić, M. M. Ristić, *Sci. Sintering*, 39(3) (2007) 229.
26. P. M. Nikolić, K. M. Paraskevopoulos, T. T. Zorba, E. Pavlidou, N. Kantiranis, S. Vujatović, O. S. Aleksić, M. V. Nikolić, T. B. Ivetić, S. M. Savić, N. J. Labus, V. D. Blagojević, *Sci. Sintering*, 39(3) (2007) 223.

27. D. T. Luković, P. M. Nikolić, S. S. Vujatović, S. M. Savić, D. B. Urošević, Sci. Sintering, 39(2) (2007) 161.
28. S. M. Savić, O. S. Aleksić, P. M. Nikolić, D. T. Luković, Sci. Sintering, 38(3) (2006) 223.
29. T. B. Ivetić, M. V. Nikolić, P. M. Slankamenac, M. B. Živanov, D. M. Minić, P. M. Nikolić, M. M. Ristić, Sci. Sintering, 39(3) (2007) 229.
30. T. B. Ivetić, M. V. Nikolić, P. M. Nikolić, V. D. Blagojević, S. Đurić, T. V. Srećković, M. M. Ristić, Sci. Sintering, 39(2) (2007) 153.
31. M. V. Nikolić, D. T. Luković, S. M. Savić, V. D. Blagojević, P. M. Nikolić, Sci. Sintering, 33(3) (2004) 165.
32. P. M. Nikolić, D. T. Luković, S. M. Savić, D. B. Urošević, S. Đurić, Sci. Sintering, 35(3) (2003) 147.
33. P. M. Nikolić, D. V. Radović, K. T. Radulović, D. T. Luković, S. S. Vujatović, S. Đurić, Sci. Sintering, 35(1) (2003) 23.
34. E. Požega, P. Nikolić, S. Bernik, L. Gomidželović, N. Labus, M. Radovanović, S. Marjanović, Rev. Metal., 53 (2017) e100.
35. S. Bernik, M. Pribošek, in: "Proceedings of the 49th International conference on Microelectronics, Devices and Materials" Eds. M. Topič, Kranjska Gora, Slovenia: MIDEM, 2013, p. 121–126.
36. H. C. Kim, T. S. Oha, D. B. Hyun, J. Phys. Chem. Solids, 61 (2000) 743.
37. F. D. Rosi, B. Abeles, R. V. Jensen, J. Phys. Chem. Solids, 10 (1959) 191.
38. H. J. Goldsmid, Mater., 7 (2014) 2577.
39. B. S. Farag, A. M. Abouel el Soud, H. A. Zayed, S. A. Gad, J. Ovonic Res., 6 (6) (2010) 267.
40. B. M. Gol'cman, V. A. Kudinov, I. A. Smirnov, Semiconductor thermoelectric materials based on  $\text{Bi}_2\text{Te}_3$ , Nauka, Moskva, 1972. (in Russian)
41. M. T. Tritt, A. M. Subramanian, Mater. Res. Bull., 31(3) (2006) 188.
42. W. H. Joen, J. Phys. Chem. Solids, 52(4) (1991) 579.
43. P. Jianlu, L. Yefan, L. Chong, W. Zumin, L. Yongchang, L. Huijun, J. Mater. Sci. Technol., 52 (2020) 162.
44. L. Ying, Q. Jixiang, Z. Yang, L. Qing, M. Pengyan, Q. Jianhang, T. Kaiping, L. Chang, C. Huiming, J. Mater. Sci. Technol., 58 (2020) 80.
45. X. Yan, B. Poudel, Y. Ma, W. S. Liu, G. Joshi, H. Wang, Y. Lan, D. Wang, G. Chen, Z. F. Ren, Nano Lett., 2010, 10: 3373-3378.
46. E. Požega, Synthesis and characterization of bismuth and tellurium single crystals doped with selenium, zirconium and arsenic, PhD thesis, University of Belgrade, Technical Faculty Bor, Serbia, 2018. (in Serbian)
47. <https://www.fzu.cz/~knizek/pdf/ThermoelectricMaterials.pdf>

---

**Сажетак:** У циљу проучавања утицаја допирања Zr на термоелектричне особине монокристалa  $\text{Bi}_{10.17}\text{Sb}_{30.72}\text{Zr}_{0.35}\text{Te}_{58.28}\text{Se}_{0.48}$  n-типа, припремљен је ингот Брицмановом методом. Сечени и џепани узорци из различитих делова ингота испитивани су Холовим ефектом заснованим на Ван дер Пауовој методи. Прва мерења су спроведена са четири омска контакта на собној температури и добијени резултати су представљени у нашим истраживањима раније. Такође, добијена је висока покретљивост носиоца наелектрисања и на узорку са сребрним контактима на температури течног азота. Монокристал је испитиван мерењима Зебековог коефицијента ( $S$ ), мерењима проводљивости ( $\kappa$ ) и отпорности ( $\rho$ ) у опсегу температуре од 40-320°C мерачем импедансе домаће израде. Добијени монокристал има вредност фактора квалитета ( $Z$ ) од  $1.22 \times 10^{-3} \text{ K}^{-1}$  на 300°C.

---

---

**Кључне речи:** Холов ефекат, термоелектрична својства, Бриџман метода, монокристал.

---

© 2023 Authors. Published by association for ETRAN Society. This article is an open access article distributed under the terms and conditions of the Creative Commons — Attribution 4.0 International license (<https://creativecommons.org/licenses/by/4.0/>).

